Peer-reviewed version available at Atmosphere 2018, 9, 237; doi:10.3390/atmos9070237

Macro- and Microphysical Characteristics of Precipitating and Non-Precipitating Stratocumulus Clouds over Eastern China

SICONG LI YUNYING LI[1] GUORONG SUN ZHIXIAN LU

Institute of Meteorology and Oceanography, National University of Defense Technology

Nanjing, 211101, China

Abstract

Stratocumulus (Sc) is the most common cloud type in China. Sc clouds may or may not be accompanied by various types of precipitation that are representative of different macro- and microphysical characteristics. The finely resolved CloudSat data products are used in this study to quantitatively investigate the macro- and microphysical characteristics of precipitating and non-precipitating Sc (PS and NPS, respectively) clouds over Eastern China (EC). Based on statistical information extracted from the CloudSat data, Sc clouds are highly likely to occur alone, in association with liquid precipitation, or in association with drizzle over 25.65% of EC. The cloud bases of NPS clouds are higher than those of PS clouds, although the latter display higher cloud top heights and thicker cloud thicknesses. The spatial distributions of microphysical characteristics differ between PS and NPS clouds. The magnitudes of microphysical characteristics in NPS clouds are relatively small and decrease with height, whereas the magnitudes of microphysical characteristics in PS clouds are relatively large and peak in response to certain circulation patterns

[1] **Corresponding author**: Prof. Yunying Li, e-mail address: ghlyy@mail.iap.ac.cn

Founding: National Natural Science Foundation of China (No. 41475069) and the China R&D Special Fund for Public Welfare Industry (meteorology: GYHY 201306068)

and over certain terrain. The variations in microphysical characteristics in Sc clouds with height and contoured frequency by altitude diagrams (CFADs) of radar reflectivity may indicate that different microphysical processes operate in PS and NPS clouds. In NPS clouds, hydrometeor particles accumulate by coalescence as they rise; once the particles are too large to be supported by updrafts, the cloud droplets form raindrops. In PS clouds, raindrops increase continuously in size via collision-coalescence processes as they fall. The levels between 2.5 and 3.0 km represent the space where particles grow most rapidly. Particles are affected by updrafts and accumulate at levels between 2.5 and 1.0 km as height decreases.

Keywords: Stratocumulus; cloud physical characteristics; Eastern China

1. Introduction

Stratocumulus (Sc) is the most widely occurring cloud type in the atmosphere. Sc clouds cover 23% of the ocean area and 12% of the land area over the globe; thus, they cover a much greater total area than other cloud types (Han and Warren 2007). Klein and Hartmann (1993) pointed out that Sc clouds occur mainly in four world regions, and China is one of these regions.

In China and the surrounding areas, Sc clouds appear mainly in three regions. These regions are the southern slope of the Tibetan Plateau; the seas between southern Japan and the Philippines; and continental Eastern China (EC), which lies on the lee side of the Tibetan Plateau (Fig. 1). According to Yu et al. (2001), the westerlies in the lower troposphere flow around the plateau to the north and south, converge over EC on the lee side of the Tibetan Plateau, and form a rising airflow. The cloud top height is limited by the inversion layer and the divergence layer in the middle troposphere, leading to the production of Sc but not other cloud types (Li and Gu 2006). The present

study focuses solely on Sc clouds over Eastern China (20-45°N, 105–130°E) and its surrounding seas. This area is marked by a yellow rectangle in Fig. 1.

The occurrence frequency of Sc over EC peaks in January and December months, and drops to its minimum in July (Wang et al. 2014). The frequent Sc cover in cold seasons reflects shortwave radiation, leading to large negative net cloud radiative forcing (Klein and Hartmann 1993) and the lowest temperature in the EC continent compared to other regions of similar latitude (Li et al. 2004). In most of the current state-of-the-art general climate models, Sc cloud radiative effect is recognized to cause larger biases than other cloud types (Zhang et al. 2014) and there is a large uncertainty and a common underestimate of the shortwave cloud radiative forcing in EC (Zhang and Li 2013). In climate models, the parameterization of cloud properties is the critical for the prediction of the clouds response to climate change (Bony and Dufresne 2005). But whether the cloud macroscopic characteristics and microphysical process and properties can be proper described in models remains an open question. For instance, the number concentration of different hydrometeor species in some one-moment microphysics schemes are diagnosed not predicted, it is set as a constant for a given precipitation species (Lin and Colle 2011; Lin et al. 1983; Morrison et al. 2009), which is inconsistent with reality.

Sc clouds may or may not be accompanied by precipitation, which represents different macro- and microphysical characteristics (Ghate et al. 2010; Rapp et al. 2013) and different cloud radiative forcings (Stevens et al. 2015). In situ observations gathered via field experiments indicate that drizzle is commonly associated with Sc clouds (Wood et al. 2011). The formation mechanisms of liquid precipitation and solid precipitation differ significantly, so the precipitating Sc clouds discussed in this article include those that produce both liquid precipitation and drizzle. Based on

Peer-reviewed version available at Atmosphere 2018, 9, 237; doi:10.3390/atmos9070237

62 the CloudSat dataset, the statistical frequency of occurrence of precipitating Sc (PS) and non-
63 precipitating Sc (NPS) clouds in EC are 25.65% and 70.87%, respectively, and these types of clouds
64 differ significantly in terms of their macro- and microphysical characteristics.

65 This study uses CloudSat data products to investigate the macro- and microphysical
66 characteristics of both PS and NPS clouds over EC. We hope that the quantitative results presented
67 here will contribute to a better and more comprehensive understanding of the precipitation
68 mechanisms that operate in Sc clouds, in addition to providing the facts needed to validate the
69 representations of cloud microphysical processes in the relevant numerical models. Section 2
70 provides a brief introduction to the data used in this study. Sections 3 and 4 give the statistical results
71 of the macroscopic characteristics and the microphysical properties of PS and NPS clouds. Section
72 5 provides a brief summary and concludes the paper.

73 2. Data

74 This study employs cloud macro- and microphysical properties derived from CloudSat data
75 products (http://www.cloudsat.cira.colostate.edu/) that cover the period from June 2006 to
76 December 2010. The clouds detected by CloudSat are classified into eight types, specifically stratus
77 (St), stratocumulus (Sc), cumulus (Cu), altocumulus (Ac), altostratus (As), nimbostratus (Ns), and
78 deep convective (DC) clouds and high clouds. Sc clouds are defined as inhomogeneous clouds with
79 base heights less than 2.0 km above ground level, horizontal scales of 10^3 km, shallow vertical
80 extents, and liquid water paths greater than zero; they either are or are not accompanied by drizzle
81 or snow (Sassen and Wang 2007; Stephens et al. 2009).

82 The Cloud Profiling Radar (CPR) onboard CloudSat operates at 94 GHz. It is able to penetrate

optically thick clouds to detect multi-layer cloud systems, but it cannot detect thin cirrus clouds with small ice water contents (Sassen and Wang 2007; Yuan et al. 2011). The Cloud-Aerosol LIDAR and Infrared Pathfinder Satellite Observation (CALIPSO) LIDAR (CALIOP) is sensitive enough to detect the optically thin cirrus clouds that are missed by radar. Combining LIDAR and radar measurements can provide effective cloud detection and characterization due to their unique complementary capabilities (Li and Zhang 2015). In this study, we primarily employ the combined LIDAR and radar product 2B-CLDCLASS-LIDAR and the CPR product 2B-CLDCLASS whenever LIDAR data are unavailable. Both of these cloud products provide information for up to 10 cloud layers, including cloud types, cloud bases, top heights, and precipitation types (e.g., drizzle, liquid precipitation, solid precipitation, or no precipitation).

The CloudSat data products 2B-CWC-RVOD and 2B-TAU provide cloud microphysical properties, including liquid/ice water contents, liquid/ice effective radii, liquid/ice number concentrations, liquid/ice distribution width parameters, and cloud layer optical depths, and the uncertainties in the values of all of these properties in each range bin. The "bin" is the basic unit of storage in CloudSat. The resolution of each bin is approximately 1.7 km along-track by 1.3 km across-track and 240 m in the vertical direction.

The CloudSat data product 2B-GEOPROF uses the data from the CPR to determine whether the levels in the vertical direction contain significant radar echoes from hydrometeors and includes an estimate of the radar reflectivity factor for each bin (Stephens et al. 2001). The CPR cloud mask included with 2B-GEOPROF provides a confidence check on the CPR output. High values of the cloud mask represent cloud detections with lower chances of false detection; mask values greater than 30 indicate that clouds are reliably detected with an uncertainty less than 2% (Mace 2001). In

addition, we also observe a noticeable uncertainty in the bins near the surface due to the CPR surface return contaminates. Consequently, bin samples below 0.5 km and cloud mask values less than 30 are discarded in this study. However, comparisons with surface station observations, aircraft observations, and ISCCP data show that the CloudSat data products are reasonable (Austin et al. 2009; Barker et al. 2008; Protat et al. 2009; Sassen and Wang. 2007).

We gather the different macro- and microphysical properties of clouds supplied by the different CloudSat data products in each range bin, as well as the macroscopic features in the 10 cloud layers. For convenience, we establish a data set in which the cloud microphysical properties are matched with each corresponding cloud layer. The data set contains more than 10 parameters describing cloud macro- and micro-properties along the CloudSat orbit. We investigate the macro- and microphysical characteristics of PS and NPS clouds over EC using this data set. There are 1,133,712 profiles that pass through the selected region and contain Sc clouds and 1,532,235 and 2,307,487 bin samples of PS and NPS clouds, respectively. Here, we focus only on the warm rain process in Sc clouds due to the limited sample number of ice particles. In particular, the PS samples in this study represent precipitation particles that form in clouds, rather than real precipitation reaching the surface.

3. Stratocumulus Macroscopic Characteristics

Cloud macroscopic characteristics, such as the number of cloud layers, cloud top and base heights, and cloud thicknesses are key factors that affect radiation budgets, the hydrological cycle, and precipitation formation mechanisms in clouds (Minnis et al. 2001; Quante 2004). Warren et al. (1985) pointed out that it is common for Sc clouds to occur simultaneously with other cloud types

126 at different levels in the atmosphere over the same location; the effects of Sc clouds on radiation
127 budgets depend on whether other clouds are present. However, the CloudSat data indicate that Sc
128 clouds are much more likely to occur alone than to be accompanied by other cloud types over EC.
129 When Sc clouds occur with other cloud types, they are typically medium or high cloud types, such
130 as high clouds, altostratus (As), and altocumulus (Ac) (Fig 2a). The average separation distance
131 between the upper cloud level and Sc is 3.08 km. This distance may be due to the mutual exclusion
132 tendency of different low cloud types.

133 Whether Sc clouds generate precipitation is strongly influenced by the generating circulation
134 pattern, water vapor conditions, and the terrain. Figure 2b shows the spatial distribution of the
135 frequency of precipitation from Sc clouds over EC. Considering the variations in cloudiness at
136 different spatial and temporal scales, the precipitation frequency can be distributed over a 2.5°×2.5°
137 grid (Rossow et al. 1993). The frequency of precipitation from Sc clouds displays a clear north/south
138 boundary at 35°N; the precipitation frequency is relatively large to the south, where it exceeds 25%.
139 Because the soil humidity is high and evaporation is strong in the south of China, and the westerlies'
140 southern branches transport warm and wet air from the Bay of Bengal to southern China and
141 converge with the northern branches on the lee side of the plateau, most Sc clouds over southern
142 China generate precipitation, particularly the Sichuan Basin (Murakami 1981; Yeh 1950). At the
143 same latitude, the frequency of precipitation from Sc clouds is larger over the ocean (>30%) than
144 that over land areas (<30%) due to the abundance of water vapor over the ocean. There is a large
145 center of precipitation frequency located over the northeastern part of Taiwan; Sc clouds are more
146 likely to occur over this area in cold seasons, and the combined effects of northeasterly Asian
147 monsoons and landforms lead to this elevated precipitation frequency (Chen et al. 1999).

Figure 3 shows the spatial distribution of the average cloud base and top heights and thicknesses of PS and NPS clouds over EC. Given the homogeneous surface properties, the cloud bases, top heights, and thicknesses of both PS and NPS clouds are much more uniform over the ocean than over land areas. Over land areas, the base and top heights of Sc clouds increase with the terrain height. When Sc clouds occur over the ocean, most of the cloud base heights of NPS clouds are less than 1.0 km, the cloud top heights are less than 1.75 km, and the cloud thicknesses range from approximately 0.5 to 0.7 km. The cloud base heights of PS clouds are generally less than 0.75 km, the cloud top heights exceed 2.25 km, and the average cloud thickness is approximately 1.7 km. For Sc clouds over land areas, the cloud bases and top heights of NPS clouds are approximately 0.25 km higher and 0.5 km lower than those of PS clouds, respectively, at any given elevation. In summary, the cloud top heights of PS clouds are greater, the cloud base heights are lower, and the cloud thicknesses are greater than those of NPS clouds.

As shown in Fig. 3f, minima in the thicknesses of PS clouds occur over the Sichuan Basin, the Southeast Hills, and the Korean Peninsula. In these areas, the cloud top height of Sc clouds is lower because it is limited by the atmospheric boundary layer. The cloud base height relative to the ocean surface is also higher because of the higher terrain, which results in thinner Sc clouds. The abundant water vapor over the ocean also causes the average cloud thickness over the ocean to be 0.3 km greater than that over land areas at the same latitude.

4. Stratocumulus Microphysical Characteristics

4.1 Probability density function of stratocumulus microphysical characteristics

The probability density functions (PDF) of the microphysical characteristics of Sc clouds

describe how the probability of occurrence of the values of microphysical characteristics varies across a certain range of values. Figure 4 shows PDFs of the microphysical characteristics of PS and NPS clouds, including their radar reflectivity, liquid water content, liquid effective radius, liquid number concentration, liquid distribution width parameters, and cloud optical depth, as detected by CloudSat over EC. The PDFs are calculated as the ratio of the bin sample number in each interval (with the ranges of values divided into 100 equal intervals) to the total bin sample number, with which most PDFs of microphysical characteristics are normalized.

Both the identification of precipitation and the retrieval of cloud properties are based on radar reflectivity (Biggerstaff and Listemaa 2000; Smith et al. 1917). The radar reflectivity values of Sc clouds range from -30 to 20 dBz (Fig. 4a). In particular, the declared minimum detectable signal of CPR is -29 dBz; some hydrometeor layers have a backscatter cross section that generates a signal near or below -29 dBz. The PDFs of radar reflectivity for both PS and NPS clouds have a single-peaked structure. The maximum probabilities for NPS and PS clouds are located around -26 dBz and -17 dBz, respectively; the maximum probability for NPS clouds is significantly greater than that for PS clouds. The PDFs indicate that the reflectivity factors of PS clouds are greater than those of NPS clouds. Suzuki et al. (2010) noted that, in warm clouds, radar reflectivity values of less than -20 dBz, from -15 to 0 dBz, and from 0 to 15 dBz correspond to cloud particles, drizzle, and raindrops, respectively. The PDFs of radar reflectivity presented in this study corroborate this conclusion.

The PDFs of liquid water content are shown in Fig. 4b. The liquid water contents in PS clouds are significantly greater than those in NPS clouds, and the range of values is wider in PS clouds; this range reaches a maximum of over 2000 $mg \cdot m^{-3}$ (not shown). In NPS clouds, most of the liquid

191 water content values do not exceed 500 $mg \cdot m^{-3}$, and the maximum probability of occurrence of
192 approximately 14% occurs near the 200 $mg \cdot m^{-3}$ level. The PDFs of the liquid number
193 concentrations associated with both PS and NPS clouds shown in Fig. 4c are right-skewed, nearly
194 normal distributions with weak probability peaks near 50 cm^{-3}. The maximum probability in PS
195 clouds is approximately 6.0% and is located near 80 cm^{-3}. In NPS clouds, the maximum probability
196 of up to 7.3% is located near 73 cm^{-3}.

197 Figure 4d shows the PDFs of the liquid effective radius in both PS and NPS clouds, which
198 reflect left-skewed, nearly normal distributions. However, the PDF associated with PS clouds
199 displays a much wider range of values than associated with NPS clouds. The maximum probability
200 is greater and located at a smaller effective radius in NPS clouds than in PS clouds. The liquid
201 distribution width parameter, which characterizes the varying distribution of droplet sizes, is shown
202 in Fig. 4e. The values of this parameter exceed 0.27 in both PS and NPS clouds, and the values in
203 PS clouds are generally greater than in NPS clouds. In other words, the droplet size varies more
204 strongly and has a greater spectrum width in PS clouds than in NPS clouds, which favors the
205 formation of precipitation in Sc clouds by coalescence. Considering the PDF of radar reflectivity
206 and the low coagulation efficiency when cloud droplets are smaller than 20 μm, the precipitation
207 type in Sc is dominated by drizzle.

208 Figure 4f plots the PDFs of cloud optical depths associated with PS and NPS clouds. The curve
209 for NPS clouds declines monotonically, and most of the cloud optical depth values are concentrated
210 in the range between 0 and 10. In PS clouds, the probability of occurrence decreases slowly as the
211 cloud optical depth increases from 0 to 60. Thus, the distribution of cloud optical depths in PS clouds
212 is more uniform over its range of values, and cloud optical depths are generally larger in PS clouds

than in NPS clouds.

Overall, one striking difference in the PDFs of the microphysical characteristics of PS and NPS clouds is that the ranges of values of the microphysical characteristics are wider in PS clouds than NPS clouds. The wider ranges of values mean that the PS clouds can generate both drizzle and strong rainfall, in agreement with the ground observation that the precipitation from Sc clouds varies substantially. Accurate prediction of precipitation from Sc clouds is challenging.

4.2 Spatial distributions of the microphysical characteristics of stratocumulus clouds

Figure 5 shows the spatial distributions of the average microphysical characteristics of PS and NPS clouds, including the liquid water path, liquid number concentration, and liquid effective radius, over EC. All of the values of the microphysical characteristics of Sc clouds are larger in the precipitating cases than the non-precipitating cases. The cloud liquid water path is calculated by integrating the liquid water content through the cloud column. As shown in Figs. 5a and 5d, the liquid water path in NPS clouds decreases as latitude increases over land areas; the liquid water path over the Sichuan Basin is greater than over its surroundings. The ocean from south of the Korean Peninsula to the northwestern Pacific (not shown) displays the largest liquid water path values because the Kuroshio Current causes the ocean surface temperature to be warmer; thus, the atmospheric stratification is unstable in this area, which favors the vertical transport of water vapor. Conversely, the peak liquid water path value in PS clouds appears over the ocean south of 30°N, where the frequency of precipitation from Sc clouds is large. The liquid water path in PS clouds is larger over the ocean than land areas at the same latitude.

The distributions of the liquid number concentration (Figs. 3b and 3e) and the liquid effective

radius (Figs. 3c and 3f) display similar spatial patterns. For the NPS clouds, both of these microphysical characteristics decrease with latitude. There is little difference in the distributions of microphysical characteristics between the ocean and land areas at the same latitude. For PS clouds, the liquid number concentration over land areas is generally greater than that over the ocean, perhaps because the aerosols produced by anthropogenic activity over land areas act as cloud condensation nuclei and increase the cloud drop number concentration (Twomey 1974). The peak liquid number concentration values over the Sichuan Basin correspond to the highest values of the aerosol optical depth in China (Luo et al. 2014). Peaks in the liquid effective radius of PS clouds appear over the Sichuan Basin, the Southeast Hills, and the Korean Peninsula. These peaks may occur due to the increase in ascending motion driven by high elevations, which result in larger precipitation particles in these areas.

4.3 Vertical distributions of the microphysical characteristics of stratocumulus clouds

The internal vertical structure of Sc clouds provides insight into the relevant microscopic properties and microphysical processes. Accordingly, we explore the vertical structure of Sc clouds over EC. Figure 6 shows the variations in the microphysical characteristics of Sc clouds with height. In this figure, pink and cyan dots indicate the microphysical characteristics of samples of PS and NPS clouds, respectively. To embody variations in microphysical characteristics with height within our large number of samples, if more than one sample is present at the same level, the mean value is calculated as to represent that level, and only the mean value is shown on the scatter plot. The vertical profiles of the microphysical characteristics are also established by polynomial fitting; the red and blue curves represent the variations in the microphysical characteristics with height in PS

and NPS clouds, respectively. Considering that the vertical extent of Sc clouds is limited to a maximum value of approximately 5.0 km (Figs. 3b and 3e) and CPR surface returns contaminate the bins near the surface, we mainly analyze the vertical variations in Sc clouds between 1.0 km and 5.0 km.

In NPS clouds, the cloud liquid water content is evenly distributed in the vertical direction, and the values change slightly with increasing height. The average liquid water content is consistently located at approximately 150 $\mathrm{mg \cdot m^{-3}}$ in each level (Fig. 6a). Below 4.0 km, the liquid number concentration decreases monotonically (Fig. 6b) as height increases. The liquid effective radius increases from approximately 9.5 μm to 10.5 μm (Fig. 6c).

In PS clouds, the liquid water content, liquid number concentration, and liquid effective radius all decrease rapidly as the height increases. The maximum values of the liquid water content appear at the bottoms of Sc clouds. The variations in the liquid effective radius in PS clouds are similar to those in NPS clouds above 4.0 km. In view of the variations in microphysical characteristics with height in NPS and PS clouds, we infer that the hydrometeor particles in NPS clouds increase due to coalescence as they rise; the particle size is smaller and increases slowly through this process. When the hydrometeor particle size is large enough that the particles are no longer supported by updrafts, the cloud droplets form raindrops and fall as NPS clouds transform into PS clouds. As they fall, the raindrops increase continuously in size as small hydrometeor particles aggregate, resulting in an increase in the average liquid effective radius with decreasing height. To this effect, collision-coalescence processes play an important role in the formation of larger liquid drops. As raindrops collide with each other, they may break apart and generate greater quantities of small drops at the bottoms of Sc clouds. Dry air intrusions at high levels evaporate small water drops, so the liquid

277 number concentration increases with decreasing height in both cases. Additionally, in both PS and
278 NPS clouds, the sample distributions of the microphysical characteristics of Sc clouds is more
279 discrete above 4.5 km; this observation may be caused by the limited quantity of samples at this
280 height level.

281 Yuter and Houze (1995) found that the statistical distributions of storm properties can be
282 conveniently summarized in the form of contoured frequency by altitude diagrams (CFADs).
283 CFADs reflect the frequencies of storm properties normalized in each geometric height bin at the
284 cost of increasing the percentages at the tops of storms, where there are relatively few data points
285 (Yin 2013). In this study, we represent the vertical structure of Sc clouds by the CFADs of radar
286 reflectivity but normalize them by the total number of samples at all levels (Fu et al. 2003), as shown
287 in Fig. 7. The solid black lines in the figure connect the points at different heights that display the
288 maximum frequencies. These lines (here called the "cloud profiles") represent the basic
289 characteristics of Sc clouds. The cloud profiles differ markedly between PS and NPS clouds.

290 Figure 7 displays the CFADs of the radar reflectivity values of NPS (a) and PS (b) clouds,
291 respectively. In NPS clouds, most of the radar reflectivity values fall between 0.5 and 3.5 km, with
292 values ranging from -30 to -20 dBz. The NPS cloud profile is effectively stable with increasing
293 height above 0.5 km, and the maximum frequency in each level generally remains at -25 dBz. In
294 effect, the vertical distribution of cloud droplets is uniform in NPS clouds. The radar reflectivity of
295 PS clouds is consistently greater than -28 dBz, and most of the radar reflectivity measurements
296 range from -25 to 5 dBz and are below 4.0 km (Fig. 7b). Above 3.0 km, the PS cloud profile is very
297 similar to that of NPS clouds, but it increases rapidly as the height decreases from 3.0 to 2.5 km.
298 This change may imply that these levels favor the growth of hydrometeors by the collision-

coalescence process. The cloud profile roughly remains at -18 dBz from 2.5 km to 1.0 km, which suggests that the speed of increase in the hydrometeor particles slows down. At these levels, the terminal velocity of drops increases with drop size; however, hydrometeor particles accumulate due to updrafts in the clouds, decreasing the rate of change in the liquid number concentration with height in PS clouds relative to NPS clouds (Fig 6b). Further, the cloud profiles rapidly increase, exceeding 0 dBz, below 1.0 km in both PS and NPS clouds, where the radar reflectivity is contaminated by surface clutter echoes.

5. Summary

The macro- and microphysical characteristics of PS and NPS clouds over EC from June 2006 to December 2010 are quantitatively analyzed in this study using CloudSat data. We observe significant differences in the macro- and microphysical characteristics, as well as microphysical processes, between PS and NPS clouds.

The statistical properties of the macroscopic characteristics show that Sc clouds are much more likely to occur alone over EC, and the associated precipitation frequency is approximately 25.65%. However, when Sc clouds occur with other cloud types, altostratus (As), altocumulus (Ac), and high clouds are most common. The frequency of precipitation from Sc clouds is greater south of 35°N than over the northern part of the study region. The precipitation frequency over the ocean is also greater than that over land areas at the same latitude. The cloud tops of PS clouds are higher, the cloud bases are lower, and the cloud thicknesses are greater than those of NPS clouds.

We also analyze the spatial distributions of the microphysical characteristics of Sc clouds over EC, including the liquid water path, liquid number concentration, and liquid effective radius. The

peak of the liquid water path is located over the ocean in both PS and NPS clouds, but this peak is located is farther north in NPS clouds. The liquid number concentration and liquid effective radius decrease as latitude increases in NPS clouds. In PS clouds, the magnitudes of the values of microphysical characteristics are greater over land areas than over the ocean. The spatial distributions of microphysical characteristics are strongly influenced by the generating circulation and terrain.

The variations in microphysical characteristics with height reflect the microphysical processes that operate in clouds. In NPS clouds, hydrometeor particles may accumulate due to condensation; however, they are small in size and grow slowly. The cloud liquid water content, liquid number concentration, liquid effective radius, and optical depth decrease rapidly with increasing height in PS clouds. The CFADs of radar reflectivity and the vertical distribution of the maximum radar reflectivity frequency reflect marked differences in microphysical processes between PS and NPS clouds. In NPS clouds, the maximum frequency of radar reflectivity generally occurs at -25 dBz at all levels; the vertical distributions of hydrometeor particle size and concentration are uniform. In PS clouds, the maximum frequency of radar reflectivity increases rapidly with decreasing height from 3.0 km to 2.5 km and remains nearly constant between 2.5 to 1.0 km. This result may imply that the hydrometeor particles grow primarily by the collision-coalescence process as they fall. The height between 3.0 and 2.5 km represents the region in which the particles grow most rapidly. Driven by updrafts, particle growth slows as accumulation continues between 2.5 and 1.0 km.

Although quantitative and theoretical in nature, this study may contribute to a better and more comprehensive understanding of the mechanisms by which precipitation is generated in Sc clouds and provides a workable reference for validating and improving the parameterization schemes used

342 in existing numerical models to represent the microphysical processes that occur in Sc clouds. In
343 the future, we plan to integrate the standard CloudSat data product 2C-PRECIP-COLUMN, which
344 provides accurate data on precipitation rates over the ocean, to further explore the differences in
345 microphysical characteristics between PS and NPS clouds.
346

Acknowledgements

The authors thank the CloudSat Data Processing Center (DPC); the data used in this study were obtained from the CloudSat website (http://www.cloudsat.cira.colostate.edu). This research was supported by the National Natural Science Foundation of China (grant 41475069) and the China R&D Special Fund for Public Welfare Industry (meteorology: GYHY 201306068).

Figure Captions

Fig. 1 Spatial distribution of the frequency of occurrence of Sc clouds detected by CloudSat from June 2006 to December 2010. Yellow rectangular box indicates the area of interest in this study, and the thick red contour denotes the edge of the Tibetan Plateau.

Fig. 2 (a) Conditional occurrence probabilities of Sc accompanied by six other cloud types, High clouds, altostratus (As), altocumulus (Ac), cumulus (Cu), nimbostratus (Ns) and deep convective (DC) clouds; Sc clouds occur alone in 73% of the observed cases. (b) Spatial distribution of precipitation frequency of Sc detected by CloudSat over EC.

Fig. 3 Spatial distributions of average cloud base heights (left panel), top heights (middle panel) and cloud thicknesses (right panel) of NPS (top row) and PS (bottom row) clouds over EC.

Fig. 4 Probability density functions (PDFs) of microphysical characteristics of Sc clouds, including (a) radar reflectivity, (b) liquid water content, (c) liquid effective radius, (d) liquid number concentration, (e) liquid distribution width parameter and (f) cloud optical depth detected by CloudSat over EC. Red and blue lines represent the PDFs of microphysical characteristics in PS and NPS clouds, respectively.

Fig. 5 Spatial distributions of the average microphysical characteristics of Sc clouds, including the liquid water path (left panel), liquid number concentration (middle panel) and liquid effective radius (right panel) of NPS (top row) and PS (bottom row) clouds over EC.

Fig. 6 Scatter plot of the vertical distributions of microphysical characteristics of Sc clouds. Red and blue curves represent the average vertical profiles of the microphysical characteristics of PS and NPS clouds, respectively, calculated by polynomial fitting. Red dots indicate bin samples of the microphysical characteristics of PS clouds; blue dots indicate bin samples of

375 the microphysical characteristics of NPS clouds.

376 **Fig. 7** Contoured frequency by altitude diagrams (CFADs) of the radar reflectivity of (a) NPS and

377 (b) PS clouds, normalized by the total numbers of non-precipitating and precipitating samples.

378 The solid black lines connect the points at different heights with the maximum frequencies.

379

Figures

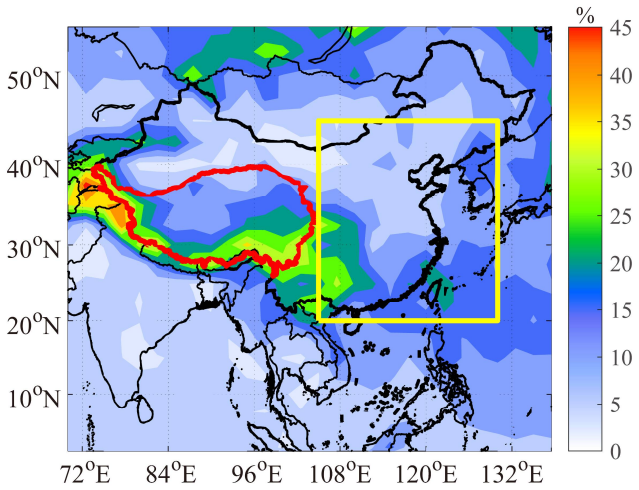

Fig. 1 Spatial distribution of the frequency of occurrence of Sc clouds detected by CloudSat from June 2006 to December 2010. Yellow rectangular box indicates the area of interest in this study, and the thick red contour denotes the edge of the Tibetan Plateau.

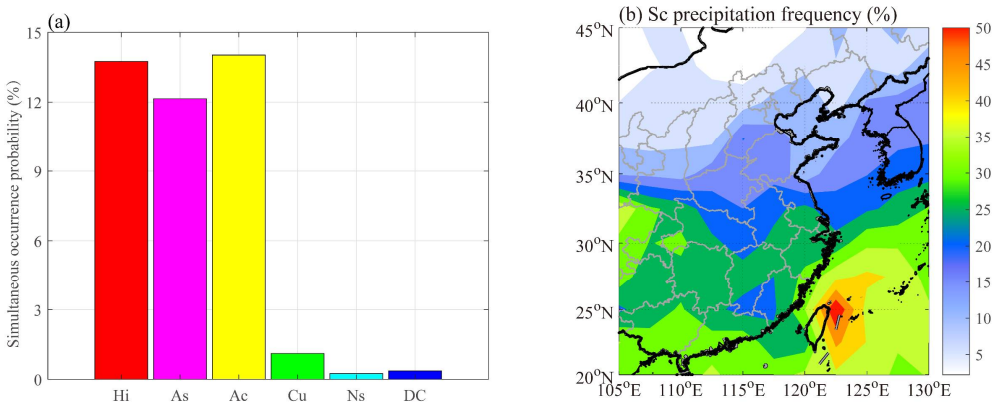

Fig. 2 (a) Conditional occurrence probabilities of Sc accompanied by six other cloud types, Hi, altostratus (As), altocumulus (Ac), cumulus (Cu), nimbostratus (Ns) and deep convective (DC) clouds; Sc clouds occur alone in 73% of the observed cases. (b) Spatial distribution of precipitation frequency of Sc detected by CloudSat over EC.

Preprints (www.preprints.org) | NOT PEER-REVIEWED | Posted: 29 March 2018 doi:10.20944/preprints201803.0248.v1

Peer-reviewed version available at Atmosphere 2018, 9, 237; doi:10.3390/atmos9070237

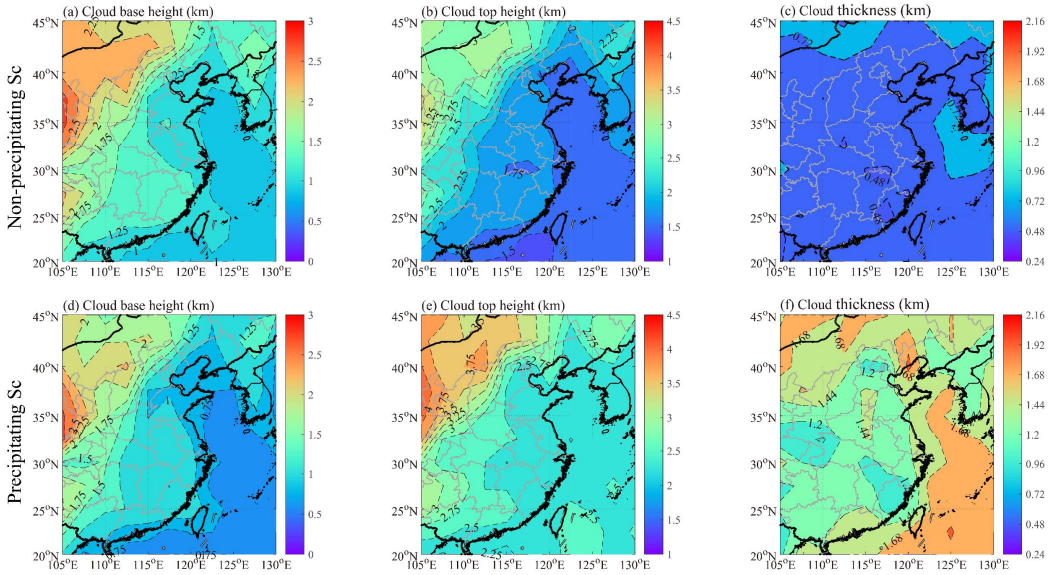

Fig. 3 Spatial distributions of average cloud base heights (left panel), top heights (middle panel) and cloud thicknesses (right panel) of NPS (top row) and PS (bottom row) clouds over EC.

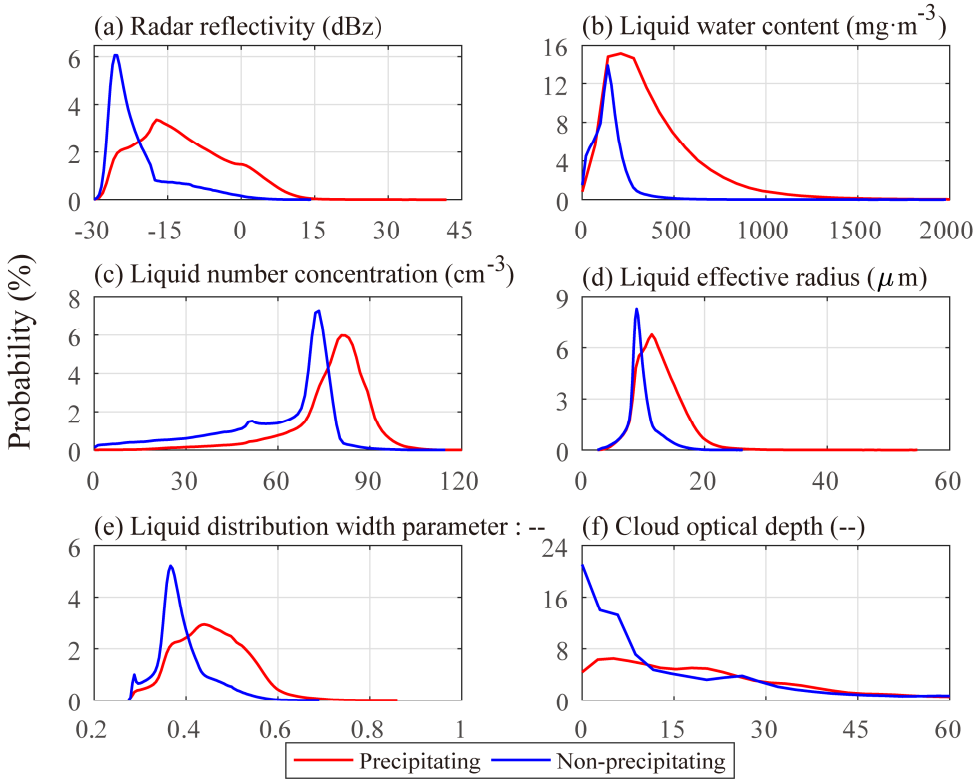

Fig. 4 Probability density functions (PDFs) of microphysical characteristics of Sc clouds, including (a) radar reflectivity, (b) liquid water content, (c) liquid effective radius, (d) liquid number concentration, (e) liquid distribution width parameter and (f) cloud optical depth detected by CloudSat over EC. Red and blue lines represent the PDFs of microphysical characteristics in PS and NPS clouds, respectively.

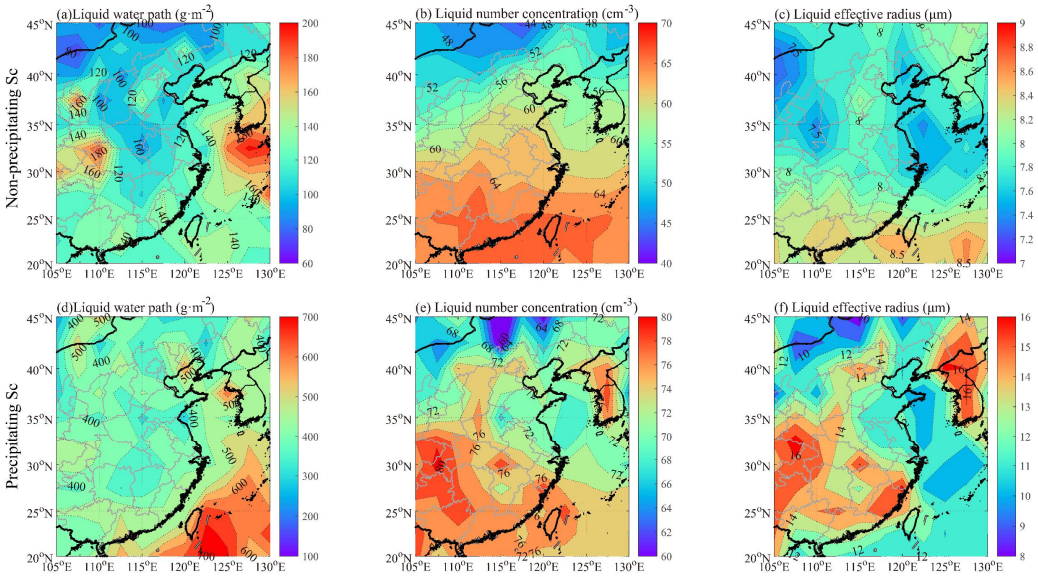

Fig. 5 Spatial distributions of the average microphysical characteristics of Sc clouds, including the liquid water path (left panel), liquid number concentration (middle panel) and liquid effective radius (right panel) of NPS (top row) and PS (bottom row) clouds over EC.

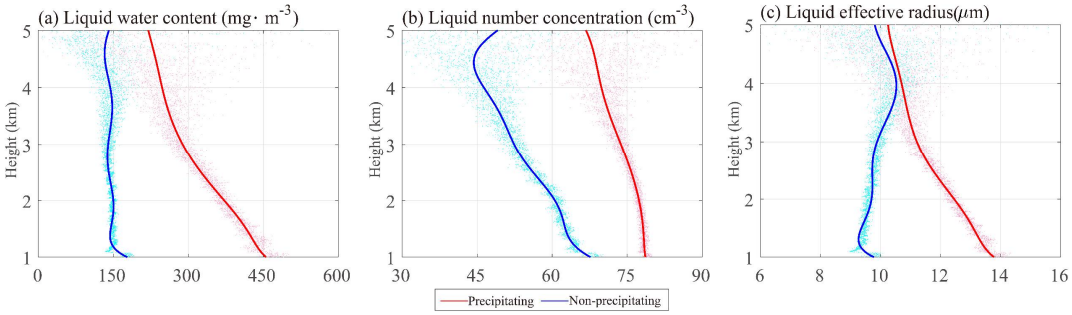

Fig. 6 Scatter plot of the vertical distributions of microphysical characteristics of Sc clouds. Red and blue curves represent the average vertical profiles of the microphysical characteristics of PS and NPS clouds, respectively, calculated by polynomial fitting. Red dots indicate bin samples of the microphysical characteristics of PS clouds; blue dots indicate bin samples of the microphysical characteristics of NPS clouds.

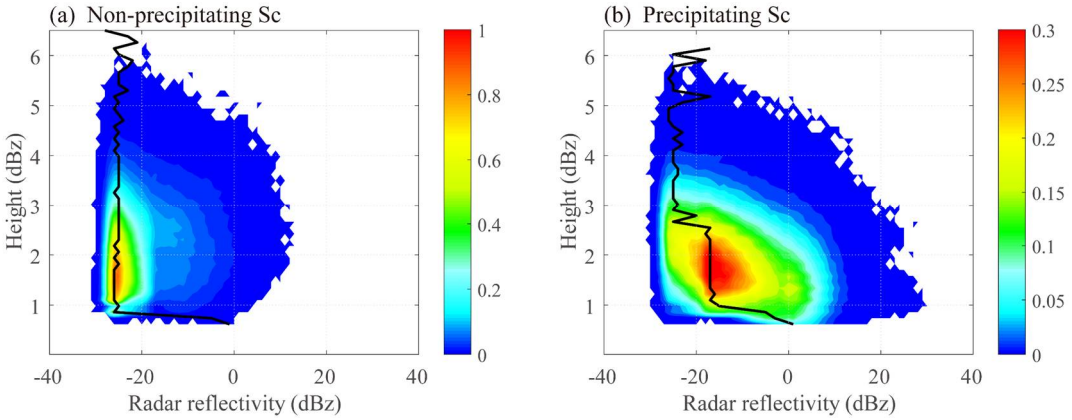

Fig. 7 Contoured frequency by altitude diagrams (CFADs) of the radar reflectivity of (a) NPS and (b) PS clouds, normalized by the total numbers of non-precipitating and precipitating samples. The solid black lines connect the points at different heights with the maximum frequencies.

Reference

Austin, R. T., Heymsfield, A. J., & Stephens, G. L. (2009). Retrieval of ice cloud microphysical parameters using the CloudSat millimeter - wave radar and temperature. *Journal of Geophysical Research Atmospheres, 114*, D00A23, doi:10.1029/2008JD010049.

Barker, H. W., Korolev, A. V., Hudak, D. R., Strapp, J. W., Strawbridge, K. B., & Wolde, M. (2008). A comparison between CloudSat and aircraft data for a multilayer, mixed phase cloud system during the Canadian CloudSat - CALIPSO Validation Project. *Journal of Geophysical Research Atmospheres, 113*, D00A16, doi:10.1029/2008JD009971, 2008.

Biggerstaff, M. I., & Listemaa, S. A. (2000). An Improved Scheme for Convective/Stratiform Echo Classification Using Radar Reflectivity. *Journal of Applied Meteorology, 39*(12), 2129-2150.

Bony, S., & Dufresne, J. L. (2005). Marine boundary layer clouds at the heart of cloud feedback uncertainties in climate models. geophys res lett 32:l20806. Geophysical Research Letters, 32(20).

Chen, T. C., Yen, M. C., Hsieh, J. C., & Arritt, R. W. (1999). Diurnal and Seasonal Variations of the Rainfall Measured by the Automatic Rainfall and Meteorological Telemetry System in Taiwan. *Bulletin of the American Meteorological Society, 80*(80), 2299-2312.

Fu, Y., Lin, Y., Liu, G., & Wang, Q. (2003). Seasonal characteristics of precipitation in 1998 over East Asia as derived from TRMM PR. *Advances in Atmospheric Sciences, 20*(4), 511-529.

Ghate, V. P., Albrecht, B. A., & Kollias, P. (2010). Vertical velocity structure of nonprecipitating continental boundary layer stratocumulus clouds. *Journal of Geophysical Research*

433 *Atmospheres, 115*, D13204, doi:10.1029/2009JD013091.

434 Hahn, C. J., and S. G. Warren, 2007: A gridded climatology of clouds over land (1971–96) and
435 ocean (1954–97) from surface observations worldwide. Carbon Dioxide Information
436 Analysis Center Tech. Rep. NDP-026E, 71 pp.

437 Klein, S. A., & Hartmann, D. L. (1993). The seasonal cycle of low stratiform clouds. *Journal of*
438 *Climate, 6*(8), 1587–1606.

439 Li, Y., & Gu, H. (2006). Relationship between middle stratiform clouds and large scale circulation
440 over eastern China. *Geophysical Research Letters, 33*, L09706,
441 doi:10.1029/2005GL025615.

442 Li, Y., & Zhang, M. (2015). Cumulus over the Tibetan Plateau in the Summer Based on CloudSat-
443 CALIPSO Data. *Journal of Climate, 29*(3), 151209140646008.

444 Li, Y., Yu, R., Xu, Y., & Zhang, X. (2004). Spatial Distribution and Seasonal Variation of Cloud
445 over China Based on ISCCP Data and Surface Observations. *Journal of the*
446 *Meteorological Society of Japan. Ser. II, 82*(2), 761-773.

447 Lin, Y. L. (1983). Bulk parameterization of the snow field in a cloud model. Journal of Applied
448 Meteorology, 22(6), 1065-1092.

449 Lin, Y., & Colle, B. A. (2011). A new bulk microphysical scheme that includes riming intensity and
450 temperature-dependent ice characteristics. Monthly Weather Review, 139(3), 1013-1035.

451 Luo, Y., Zheng, X., Zhao, T., & Chen, J. (2014). A climatology of aerosol optical depth over China
452 from recent 10 years of MODIS remote sensing data. *International Journal of*
453 *Climatology, 34*(3), 863-870.

454 Mace, G. (2001). Level 2 GEOPROF product process description and interface control document.

Nasa Jet Propulsion Laboratory.

Minnis, P., W. L. Smith, and D. F. Young, 2001: Cloud macro- and microphysical properties derived from GOES over the ARM SGP domain. In *Proceedings of the Eleventh Atmospheric Radiation Measurement (ARM) Science Team Meeting*, ARM-CONF-2001. U.S. Department of Energy, Washington, D.C. Available URL: http://www.arm.gov/docs/documents/technical/conf_0103/minnis-p.pdf

Morrison, H., Thompson, G., & Tatarskii, V. (2009). Impact of cloud microphysics on the development of trailing stratiform precipitation in a simulated squall line: comparison of one- and two-moment schemes. Monthly Weather Review, 137(3), 991-1007.

Murakami, T. (1981). Orographic influence of the Tibetan Plateau on the Asiatic winter monsoon circulation. Part I : Large-scale aspects. *Journal of the Meteorological Society of Japan, 59*(1), p40-65.

Protat, A., Bouniol, D., Delanoë, J., May, P. T., Plana-Fattori, A., Hasson, A., O'Connor E, Görsdorf U, Heymsfield, A. J. (2009). Assessment of Cloudsat Reflectivity Measurements and Ice Cloud Properties Using Ground-Based and Airborne Cloud Radar Observations. *Journal of Atmospheric and Oceanic Technology, 26*(9), 1717-1741.

Quante, M. (2004). The role of clouds in the climate system. *J. Phys. IV France, 121*, 61-86.

Rapp, A. D., Lebsock, M., & L'Ecuyer, T. (2013). Low cloud precipitation climatology in the southeastern Pacific marine stratocumulus region using CloudSat. *Environmental Research Letters, 8*(1).

Rossow, W. B., Walker, A. W., & Garder, L. C. (1993). Comparison of ISCCP and other cloud amounts. *Journal of Climate, 6*, 2394-2418

477 Sassen, K., & Wang, Z. (2007). Level 2 Cloud Scenario Classification Product Process Description
478 and Interface Control Document. technical report, Coop. Inst. for Res. in the Atmos.,
479 Colo. State Univ., Fort Collins.
480 Smith, P. L., Jr, Myers, C. G., & Orville, H. D. (1917). Radar Reflectivity Factor Calculations in
481 Numerical Cloud Models Using Bulk Parameterization of Precipitation. *Journal of*
482 *Applied Meteorology, 14*(14), 1156-1165.
483 Stephens, G. L., Vane, D. G., Boain, R., Mace, G., Sassen, K., & Wang, Z., et al. (2001). The
484 cloudsat mission and the EOS constellation: a new dimension of space-based
485 observation of clouds and precipitation. Submitted to *Bull. Amer. Meteoro. Soc.*
486 Stephens, G. L., Vane, D. G., Tanelli, S., Im, E., Durden, S., Rokey, M., … Marchand, R. (2009).
487 CloudSat mission: Performance and early science after the first year of operation.
488 *Journal of Geophysical Research: Atmospheres, 113*(D8), 2036-2044.
489 Stevens, B., Beljaars, A., Bordoni, S., Holloway, C., Köhler, M., Krueger, S., Savic-Jocic V, Zhang,
490 Y. (2015). On the Structure of the Lower Troposphere in the Summertime Stratocumulus
491 Regime of the Northeast Pacific. *Monthly Weather Review, 135*(3), 985-1005.
492 Suzuki, K., Nakajima, T. Y., & Stephens, G. L. (2010). Particle Growth and Drop Collection
493 Efficiency of Warm Clouds as Inferred from Joint CloudSat and MODIS Observations.
494 *Journal of the Atmospheric Sciences, 67*(9), 3019–3032.
495 Twomey, S. (1974). Pollution and the planetary albedo. *Atmospheric Environment (1967), 8*(12),
496 1251-1256.
497 Wang, M., Gu, J., Yang, R., Zeng, L., & Wang, S. (2014). Comparison of cloud type and frequency
498 over China from surface, FY-2E, and CloudSat observations. Paper presented at the *Proc.*

SPIE. 9259, Remote Sensing of the Atmosphere, Clouds, and Precipitation V, 925913. (November 20, 2014).

Warren, S. G., Hahn, C. J., & London, J. (1985). Simultaneous Occurrence of Different Cloud Types. *Journal of Climate and Applied Meteorology, 24*(7), 658-667.

Wood, R., Mechoso, C. R., Bretherton, C. S., Weller, R. A., Huebert, B., Straneo, F., … Bower, K. N. (2011). The VAMOS ocean-cloud-atmosphere-land study regional experiment (VOCALS-REx): Goals, platforms, and field operations. *Atmospheric Chemistry and Physics, 11*(2), 627–654.

Yeh, T.-C. (1950). The Circulation of the High Troposphere over China in the Winter of 1945–46. *Tellus, 2*(3), 173–183.

Yin, J., Wang, D., Zhai, G., & Wang, Z. (2013). Observational Characteristics of Cloud Vertical Profiles over the Continent of East Asia from the CloudSat Data. *Acta Meteorologica Sinica, 27*(1), 26-39.

Yu, R., Yu, Y., & Zhang, M. (2001). Comparing cloud radiative properties between the Eastern China and the Indian monsoon region. Advances in Atmospheric Sciences, 18(6), 1090–1102.

Yuan, J., Houze, R. A., Jr, & Heymsfield, A. J. (2011). Vertical Structures of Anvil Clouds of Tropical Mesoscale Convective Systems Observed byCloudSat. *Journal of the Atmospheric Sciences, 68*(8), 1653-1674.

Yuter, S. E., & Houze, R. A. (1995). Three-Dimensional Kinematic and Microphysical Evolution of Florida Cumulonimbus. Part II: Frequency Distributions of Vertical Velocity, Reflectivity, and Differential Reflectivity. Monthly Weather Review, 123(7), 1921-1940.

521 Zhang W., & Li J. (2013). Shortwave cloud radiative forcing on major stratus cloud regions in
522 AMIP-type simulations of CMIP3 and CMIP5 models. Adv. Atmos. Sci., 30, 884–907.
523 Zhang, Y., Chen, H., & Yu, R. (2014). Simulations of stratus clouds over eastern china in cam5:
524 sensitivity to horizontal resolution. Journal of Climate, 27(27), 7033-7052.